Photodynamic therapy for the treatment of metastatic lesions in bone: Studies in rat and porcine models

S. Burch
Ontario Cancer Institute
University Health Network
610 University Avenue
Toronto, Ontario
Canada M5G 2M9
and
Orthopaedic Biomechanics Laboratory
Sunnybrook and Women's College
Health Sciences Centre
2075 Bayview Avenue
Toronto, Ontario
Canada M4N 3M5

A. Bogaards
J. Siewerdsen
D. Moseley
Ontario Cancer Institute
University Health Network
610 University Avenue
Toronto, Ontario
Canada M5G 2M9

A. Yee
J. Finkelstein
Orthopaedic Biomechanics Laboratory
Sunnybrook and Women's College
Health Sciences Centre
2075 Bayview Avenue
Toronto, Ontario
Canada M4N 3M5

Robert Weersink
B. C. Wilson
S. K. Bisland
Ontario Cancer Institute
University Health Network
610 University Avenue
Toronto, Ontario
Canada M5G 2M9

Abstract. This study represents the first reported use of photodynamic therapy (PDT) for metastatic bone lesions and specifically, as a treatment for spinal metastases. A model of bone metastasis in rat confirmed the efficacy of benzoporphyrin derivative-monoacid-mediated PDT for treating lesions within the spine and appendicular bone. Fluorimetry confirmed the selective accumulation of drug into the tumor(s) at 3 h post-injection. 48 h post-light delivery into the vertebral body of the rat spine loss of bioluminescent signal and histological analyses of sectioned spine confirmed MT-1 tumor cell kill *in vivo* as previously confirmed *in vitro* using an established cell viability assay. Porcine vertebrae provided a model comparable to that of human for light propagation and PDT response. Histological examination of vertebrae 48 h post-PDT revealed a necrotic radius of 0.6 cm with an average fluence rate of 4.3 mW/cm^2. Non-necrotic tissue damage was evident up to 2 cm out from the treatment fiber. Results support the application of PDT to the treatment of primary or metastatic lesions within bone.
[DOI: 10.1117/1.1921887]

Keywords: photodynamic; bone; metastases; spine; dosimetry; bioluminescence; cancer.

Paper 04079 received May 18, 2004; revised manuscript received Nov. 5, 2004; accepted for publication Dec. 20, 2004; published online May 26, 2005. This paper is a revision of a paper presented at the SPIE conference on Optical Methods for Tumor Treatment and Detection: Mechanisms and Techniques in Photodynamic Therapy XIII, Jan. 2004, San Jose, California. The paper presented there appears (unrefereed) in SPIE Proceedings Vol. 5315.

1 Introduction

Over 100,000 bone metastases are identified in North America each year and of those an estimated 30–40,000 cases of metastatic breast cancer lesions occur in the spine.[1,2] Yet, despite this alarming statistic, the frontline approach for treating such cancers remains irrefutably unsatisfactory and the related diagnosis is often met with a poor prognosis. Presently, radiation therapy (RT) is considered the mainstay of treatment for ambulatory patients, whereas surgery is reserved for those experiencing collapse or neurological compromise. However, RT provides only limited relief from pain, composite to cord compression, offers no stability to the spine, and can adversely affect the capacity for soft tissue to repair following treatment. This in turn translates into a threefold increase in morbidity and mortality following surgical intervention.[3–5] Photodynamic therapy (PDT) is a novel, nonionizing therapy that can directly target interstitial, metastatic lesions. PDT works by delivering an excitation light of specific wavelength to a targeted tissue containing a photolabile compound, or photosensitizer. The photosensitizer is activated by the light, which in turn initiates a photochemical reaction that leads to the generation of reactive oxygen species (ROS), predominantly singlet oxygen ($^1O_2$). $^1O_2$ can kill cells directly or damage the neo-vasculature of targeted aberrant tissue.[6–8]

Address all correspondence to Stuart K. Bisland, Princess Margaret Hospital/OCI, Room 7-307, 610 University Avenue, Toronto, Ontario, Canada M5G 2M9. Tel.: 416-946-4501-5916; Fax: 416-946-6529; E-mail: sbisland@uhnres.utoronto.ca

1083-3668/2005/$22.00 © 2005 SPIE

Specificity of treatment is facilitated by the direct placement of an optical fiber cable adjacent to or within the lesion. Pithily, PDT promises to offer targeted tumor ablation without collateral damage to nearby spinal cord and little obstruction to subsequent wound repair processes within soft tissue. To our knowledge there are no prior published reports of this therapy being used in a metastatic bone model despite its use in lung,[9,10] intraperitoneal,[11] and prostate cancer.[12] In order to substantiate our hypothesis that PDT could be used effectively to treat metastatic disease in bone, we investigated this with both *in vitro* and *in vivo* models using the human metastatic breast cancer cell line, MT-1.[13] A bioluminescent metastatic model in the nude rat was developed to facilitate the localization, targeting, and progression of lesions prior to and following PDT treatment. The transmittance of irradiating light through porcine vertebrae was also evaluated as an approach for discerning light dosimetry in a model comparable to that in the human. These findings highlight the fact that PDT can be delivered into bone and further support the notion that PDT will provide a valuable alternative and/or adjunct to RT in the treatment of bone cancer without the preclusion of subsequent percutaneous vertebropasty or kyphoplasty, either for first time treatments or repeat following metastatic recurrence.

2 Materials and Methods

2.1 *Rat Model*

2.1.1 *Cells*

MT-1 cells, a human breast cancer cell line, were kindly provided by Dr. O. Engebraaten, Norwegian Radium Hospital, Oslo, Norway. Cells were grown and maintained in Roswell Park Memorial Institute (RPMI) 1640 media containing 100 U/mL penicillin and 0.1 mg/mL streptomycin with 10% fetal bovine serum (Gibco, Grand Island, NY, USA) at 37 °C, 5% CO_2/95% O_2. At 70–80% confluence cells were resuspended into free RPMI and harvested using a 0.05% trypsin–0.05 mM ethylenediamine tetra-acetic acid (EDTA, Gibco) solution. A cell suspension was prepared at 2×10^5 cells/mL and plated into chambered, borosilicate coverglass slides (LabTek®, Nalge Nunc International Corp, Naperville, IL, USA).

2.1.2 *Benzoporphyrin derivative (BPD-MA; Verteporfin™) uptake into cells*

The uptake of benzoporphyrin-derivative monoacid [BPD-MA; Verteporfin™, QuadraLogic Technologies, Vancouver, Canada; 1 μg/mL in phosphate buffer solution (PBS; 45 mM Na_2HPO_4, 5 mM NaH_2PO_4, and 0.15 M NaCl, *p*H 7.4)] into MT-1 cells was visualized using epi-fluorescence microscopy (Zeiss AxioVert 200 M; $\lambda_{ex}/\lambda_{em}$=BandPass 485/20 nm and LongPass 590 nm, respectively) and recorded using a charge-coupled camera (CoolSnap HQ; Photometrics, Roper Scientific, MD, USA) attached to the microscope.

2.1.3 *BPD-MA detection in vivo*

BPD-MA (0.25 mg/kg in PBS) was administered intravenously (i.v.) into 10 athymic, nude *rnu*/*rnu* rats (150–180 g, Harlan Sprague Dawley Indianapolis, IN, USA) through the tail vein. Animals were then euthanized upon CO_2 inhalation at 15 min, 3 h, 6 h, and 24 h post-injection and samples (n =2/time point) of serum, spine, and spinal cord were harvested. Control animals that did not receive BPD-MA injection were sacrificed 15 min post-saline injection (of equivalent volume). The spine was fixed in 10% formalin for 7 days, decalcified in 10% formic acid for an additional 7 days prior to quantitative analysis of BPD-MA fluorescence using fluorescent microscopy. Control studies confirmed that BPD-MA and its corresponding fluorescence were unaffected by the formic acid treatment (not shown). Spectrofluorimetric (Photon Technology International, London, ON, Canada) measurements of BPD-MA uptake into blood serum and spinal cord was performed on solubilized samples using a technique previously described in our laboratory.[14]

2.1.4 *Cell viability assay in vitro*

The PDT-induced cell kill was assayed in clear, flat-bottomed 96 well microplates (Corning Inc., Life Sciences, Acton, MA, USA) using the Sulphorhodamine B (SRB) viability assay.[15] 200 μL of a 2×10^5 MT-1 cells/mL suspension was added to each well. Once attached, BPD-MA was added to give a final concentration of 1 or 10 μg/mL and 8 h later, cells were irradiated with 150 mW of 690 nm laser (Model LFI 4532, Wavelength Electronics, London, ON, Canada) light for a total light dose of 100 or 25 J/cm^2. At 24 h following PDT treatment, the growth media was removed from the wells and the cells rinsed with sterile PBS to remove the dead cell population. The remaining cells were fixed in 10% trichloroacetic acid (TCA; 100%) at 4 °C for 1 h. After fixation, the wells were left to dry at room temperature before adding 50 μL of 0.4% (w/v) SRB solution (in 1% acetic acid). Cells were stained for 30 min at room temperature prior to rinsing ($\times5$) with 1% acetic acid and dried. The cell bound SRB was finally precipitated out using 100 μL unbuffered Tris solution (Sigma; Trizma base; *p*H 10.5 and the resulting absorbance read at 540 nm (with 690 nm background subtraction) using a microplate spectrophotometer (Titertek Multiskan® MCC/340). Results are expressed as normalized values to the controls (cells exposed to light without BPD-MA). All reagents used in this assay were purchased from Sigma-Aldrich Canada Ltd. (Oakville, Ontario, Canada) unless otherwise stated.

2.1.5 *Spinal metastases model*

Ten nude *rnu*/*rnu* female rats (4–6 weeks of age) were anaesthetized using halothane/O_2 (2%/3.5 L respectively) then injected with MT-1 cells (2×10^6 in 200 μL) into the left ventricle using a 1 mL syringe with a 26 G needle. Pulsatile blood within the injection syringe confirmed that the needle was in the left ventricle. Following the injection, animals were immediately recovered and returned to their cages with free access to food and water. Animals were examined 14 and 21 days post-injection for signs for paralysis and/or cachexia and the progression of metastases assessed using fine detail radiography (faxitron™). By 21 days, most animals displayed profuse bony metastases within the spine, upper femur, tibia lower mandible, and occasionally in the shoulder or humerus. Some animals were excluded from the study due to the development of extensive tumor burden outside the spine (most notably the pericardium) or due to a debilitating loss of body weight (>50%). After PDT treatment, vertebrae and long

bones were harvested and fixed in 10% formalin for 7 days. Micro-CT images of lytic lesions within the spine and/or femur were obtained prior to decalcification in 10% formic acid for 7 days and the presence of tumor within these sites confirmed histologically from haematoxylin and eosin-labeled paraffin sections using light microscopy.

2.1.6 *Co-transfected of MT-1 cells for stable expression of the luciferase gene*

All transfection reagents were purchased from Promega (Madison, WI, USA). MT-1 cells were subject to co-transfection using dioctadecylamidoglycylspermine-trifluoroacetate salt (Transfectam; E1231) with plasmid DNA containing the luciferase gene of the fire-fly (*Photinus pyralis*, pGL3 control vector E1741) and a plasmid containing the neomycin resistance gene (PCI-Neo, E184, Promega). Luciferin; Stable transfects of Luciferase-expressing MT-1 cells (MT-1^{Luc}) were confirmed by growing cells in the presence of G-418 antibiotic (100 μg/mL; G-418 sulphate) for 10 days, at which time those colonies expressing the highest bioluminescent signal were isolated and cultured. Bioluminescent signal was analyzed using the IVIS Bioluminescent Imaging system from Xenogen Corp (Alameda, California, USA). Bioluminescence of the luciferase gene was initiated following the addition of Luciferin substrate (25 μM; beetle, potassium salt anhydrous, E1603) to cells *in vitro* or 30 mg/kg i.p. *in vivo*. *In vitro*, 10 μL of Luciferin stock (0.5 mM in PBS) was added to MT-1^{Luc} cells containing 190 μL of growth media (without phenol red). The plates were gently agitated and placed into the IVIS. *In vivo*, MT-1^{Luc} (2×10^6 in 200 μL) were injected intracardially (see previous discussion) and the resulting bioluminescent signal analyzed at time points post-treatment (0–48 h). Bioluminescent signal was captured as the absolute total flux (photons/steradian/cm^2) emitted within a 5 min integration time using the Living image™ software and plotted against time.

2.1.7 *PDT treatment of bone metastases*

At day 21 post-injection, tumor-bearing animals ($n=43$; *rnu*/*rnu*, 4–6 weeks of age) were anesthetized with 2% halothane/air mixture and placed into a custom made radiolucent, stereotactic jig in the left lateral decubitus position. Because lesions within the vertebral bodies could not be detected by fine detail radiography, histological analysis of bone taken from 10 animals used in establishing the metastatic model (see previous discussion) was also used to confirm that for those animals with tumor, by 21 days most vertebrae contained metastases and the T12 and L4 vertebrae were selected as representative levels for treatment. An 18 G needle was placed onto the cortex of the targeted vertebrae or long bone with the use of a mini C-arm image intensifier. BPD-MA was administered intravenously at a dose of 2 mg/kg prior to the administration of the light dose. Drug light intervals included 1, 3, and 24 h 690 nm laser light (150 mW output) was delivered via an optical fiber (200 μm o.d.) inserted through the needle. Light doses ranged from 25 to 150 J. The effects of different drug light intervals and different light doses using a fixed drug concentration were evaluated immunohistochemically using the TdT-mediated dUTP Nick-End Labeling (TUNEL) assay (ApoDirect, Promega, Madison, WI) and H&E staining to identify apoptotic cells and necrotic cells, respectively. A human, horseradish peroxidase labeled primary antibody to the endothelial growth factor receptor (EGF-r; Invitrogen Inc., Paisley, Scotland) and keratin staining provided reliable labeling of MT-1 or MT-1^{Luc} tumor cells within bone marrow *in situ*. The area of effect was quantified using a Nikon slide scanner and Image Pro™ software and the relative decrease in viable MT-1^{Luc} cells following PDT was quantitatively assessed for each targeted lesion based on the change in bioluminescence signal before and after treatment. The use of the mini-C-arm fluoroscopic imager and the stereotactic frame, allowed the position of the optical fiber (and hence the target for PDT) and the bioluminescence signal from that location to be correlated precisely.

2.1.8 *Statistical analysis*

Statistical significance between treatment and control groups was tested using one-way analysis of variance (ANOVA) for 95% confidence intervals with Bonferroni correction for multiple comparions of group means.

2.2 *Porcine Model*

2.2.1 *Animal model*

Five female, Landrace pigs (46–53 kg body weight) were used. Animals were taken off solid food 18 h prior to surgery. Anaesthesia was induced following i.v. bolus injection of Ketamine (Ketalean®, 15 mL; 30 mg/kg, BiMeda-MTC, Animal Health Inc., Cambridge, Canada), the animals were intubated and maintained under anaesthetic [2% isoflurane (Abbott Laboratories Ltd., Saint-Laurent, Quebec, Canada)/0.4 FIO_2] with assist-controlled ventilation (12 breaths/min, 600 cc tidal volume) throughout the surgery. Physiological measurements included mean arterial blood pressure, heart rate, partial oxygen saturation, and rectal temperature. Animals were hydrated throughout the procedure with 0.9% sodium chloride solution (10 mL/min; Baxter Corporation, Toronto, Canada). Once stable, the animals were placed prone onto a custom-designed, radiotranslucent gurney to allow free access for circumferential 3-D cone beam computer tomography (CBCT; see the following discussion). Two laproscopic incisions (4 cm) were made using a scalpel through the skin and underlying muscle proximal to the transverse processes (left and right) of vertebrae L1 and L2. A channel (~2 mm diameter) was made through each pedicle of both the left and right transverse processes into the vertebral bodies of L1 or L2. Channels within the left and right pedicles were orientated approximately 70–90% planar angle to each other through which closed-ended, optically translucent catheters were placed. The fluence detector probe(s) (400 μm silicon with spherical, isotropic tip) and emitting fiber(s) (2 cm cylindrical diffusing tip, 400 μm diameter silicon) were subsequently inserted into the catheters.

2.2.2 *Imaging acquisition*

Guidance for placement of the probes was afforded by fluoroscopy and CBCT imaging in the lateral and anterior/posterior aspects. The precise coordinates (x,y,z) for each probe within the vertebrae were discerned from reconstructed CT images. We acquired over 200 projections across 180° in 60 s with high resolution (1024×768 pixels) per projection at

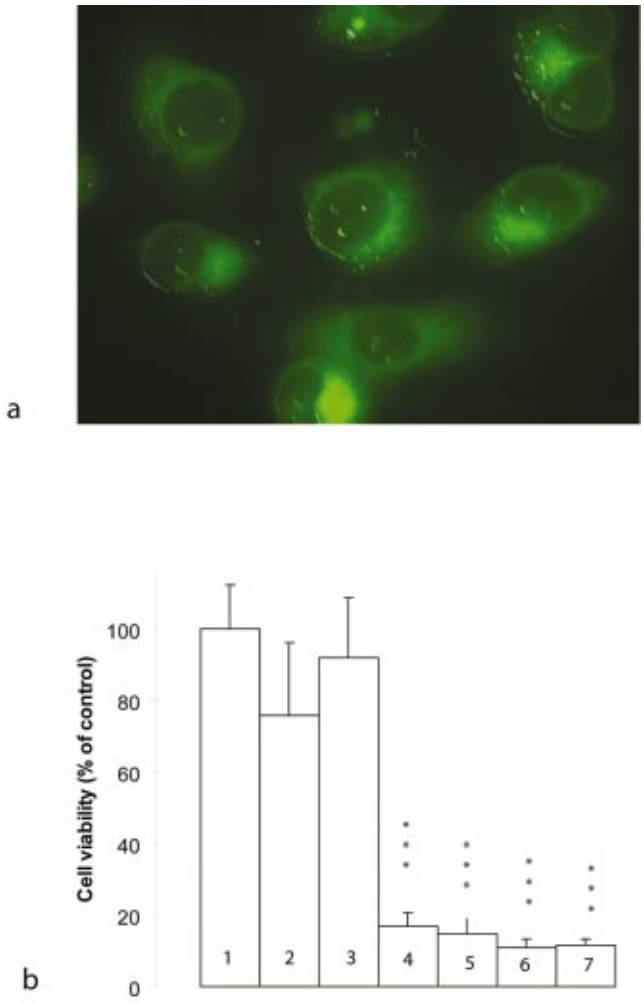

Fig. 1 Fluorescence microscopy images showing the presence of BPD-MA predominantly localized to perinuclear sites within the cytosol of cells after 45 min incubation at 37 °C, 95% O_2. Magnification 63×. (a) SRB assay confirms the sensitivity of MT-1^{Luc} cells to BPD-MA-PDT using 1 μg/mL BPD-MA and 25 J/cm^2 (lane 4) or 100 J/cm^2 (lane 6) which was not significantly altered using 10 μg/mL BPD-MA and 25 J/cm^2 (lane 5) or 100 J/cm^2 (lane 7) (b) Results are expressed as percent viability of untreated cells (lane 1) with 10 μg/mL BPD-MA (Lane 2) or 100 J/cm^2 (Lane 3) light treatment alone included as controls.

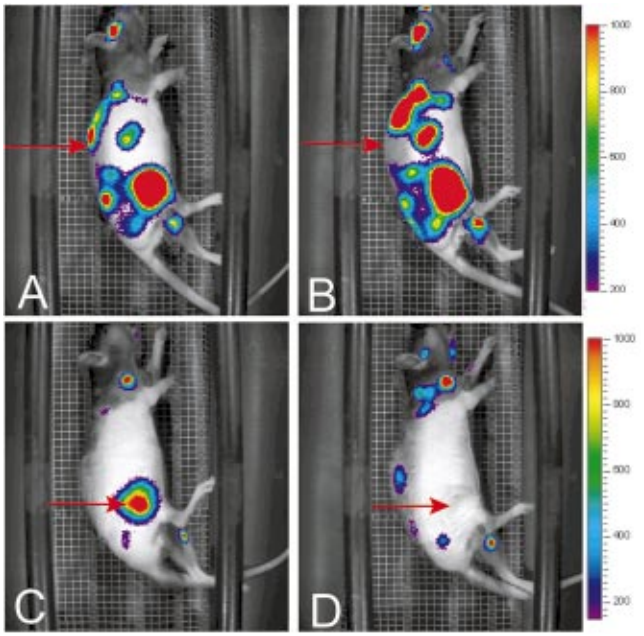

Fig. 4 Bioluminescent MT-1^{Luc} lesions in the spine and femur of rnu/rnu rats (see arrows) before (a and c) and 48 h after (b and d) PDT with 1 μg/mL, i.v. BPD-MA, followed 3 h later with 150 J/cm^2 irradiance. The bioluminescence signal from lesions is considerably reduced and in some cases the signal is lost entirely.

388 μm/pixel that were reconstructed by cosine reconstruction, medium filter with 0.5 mm resolution (512×512×384; 400 μm voxels) using a Pentium 4 processor and acquisition time of approximately 6 min. CBCT consisted of a Varian 43030 A flat panel imager mounted on a Siemens PowerMoBIL™ Isocentric C-arm. Fluoroscopy involved spot film imaging of orthogonal pair images at 125 kVp, 4.3 mA at 0.5 resolution projections (1024×768 pixels).

2.2.3 *Light dosimetry and analysis*

Once in place, irradiating light (150 mW/cm; 690 nm) was transmitted into each of the vertebrae, L1 and L2 and light dosimetry studies were conducted by retracting the isotropic fluence detector probe and catheter out of the vertebral body towards the pedicle in ten incremental movements each 2.5 mm apart. Measurements of fluence rate (Φ; mW/cm^2) at each of the ten points within the vertebrae were made using a four-channel PMT system as the probe was retracted. The subsequent delivery of PDT into the vertebrae resulted in a necrotic lesion, the radius of which (r_n) was measured on histological sections along the short axis of the treatment area and paired with the actual Φ at the necrotic/non-necrotic boundary. We were then able to confirm the average Φ obtained at r_n during the *in vivo* light dosimetry measurements. Although the intention was to cut the sections normal to the length of the treatment fiber, this was not always possible, in which case the shorter axis was considered the more accurate measurement of r_n. When measurements were not available at precisely r_n, $\Phi(r_n)$ was extrapolated from measurements at separations surrounding r_n.

Optical properties of the tissue were estimated by fitting the fluence rate measurements to an analytical diffusion model for a linear diffuser[16]

$$\Phi(r) = \frac{S_0 e^{-(r/\delta)(\pi\delta/2r)^{1/2}}}{2\pi\mu_a\delta^2}, \qquad (1)$$

where r is the radius from the diffusing fiber, δ is the penetration depth, μ_a is the absorption coefficient of the tissue, and S_0 is the incident power per centimeter of fiber. This model was also used to estimate the extent of PDT-induced damage for different light doses. The threshold Φ will remain the same regardless of the S_0, with r_n, increasing with higher treatment power. The change in r_n can be estimated by taking the ratio of Eq. (1) for two different values of S_0, i.e., $\Phi(r_n)/\Phi(r_n')$ for S_0 and S_0', respectively. Equation (1) can be rearranged to decifer r_n as shown by

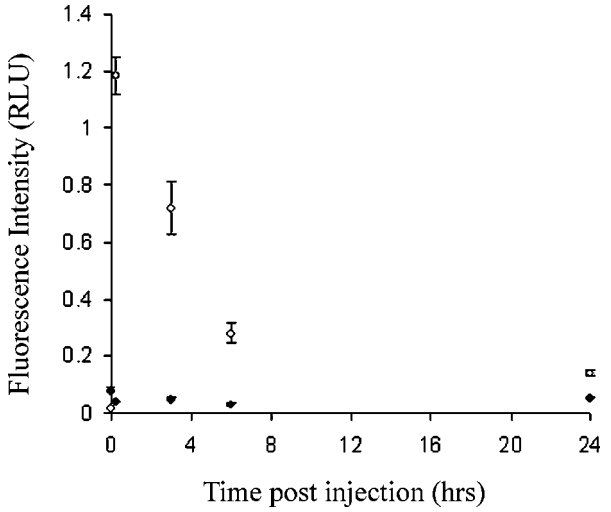

Fig. 2 Pharmacokinetic uptake of BPD-MA into blood serum and the spinal cord. BPD-MA is rapidly cleared from the serum within 6 h i.v. post-injection. Uptake into the spinal cord is considerably less with a maximum reached at 3 h post-injection.

$$r_n' = \left[(\delta/2\pi)^{1/2} \ln\left(\frac{S_0'}{S_0}\right) + \sqrt{r_n} \right]^2 . \qquad (2)$$

2.2.4 *Preparation of BPD-MA*

BPD-MA was supplied as a dry powder. The powder was reconstituted into 7 mL of sterile de-ionized water, filtered (0.45 μm Millipore filter) and added into 23 mL of 5% dextrose solution (Baxter Corporation, Toronto, Canada). Preparation was conducted on the day of the experiment.

2.2.5 *BPD-MA-PDT in the spine*

In order to negate the inflammatory/allergic reaction of the pigs to the photosensitizing agent, BPD-MA, benadryl® (Warner-Lambert Company, Morris Plains, NJ, USA) was administered (2 mg/kg i.v. bolus) 5 min before BPD-MA and similarly, to avoid precipitation of the BPD-MA out of solution, the saline i.v. infusion was flushed with 5% dextrose solution. BPD-MA (0.33 mg/kg; ~6 mg/m^2) was subsequently co-injected as a slow infusion (1.5 mg/min for 10 min) together with the dextrose. At 30 min or 1 h post-BPD-MA administration, light (150 J/cm, 150 mW/cm, 690 nm) was delivered to the L1 and/or L2 vertebral bodies for a total duration of 36 min/treatment.

2.2.6 *Post-operative care*

After PDT was given, the probes were removed and the small incisions through the muscle and skin sutured closed (4.0 braided vycril and 2.0 prolene, respectively; Ethicon Inc., Johnson and Johnson Co., Somerville, NJ, USA). The animals were recovered to the point of being able to stand unaided before being given buprenorphine analgesic (Buprenex®, 0.01 mg/kg, i.m. bolus) and antibiotic (2.5 mL i.m. bolus of 1500 I.U. Duplocillin® LA; Intervet Canada Ltd., Whitby, Canada). Repeat injections of analgesic were given twice daily.

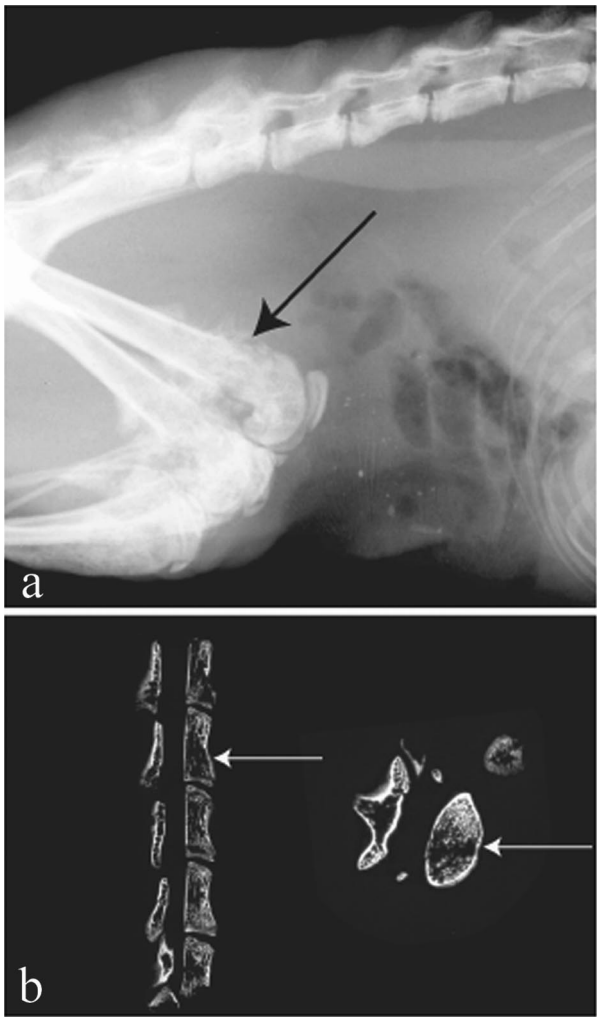

Fig. 3 Osteolytic lesions secondary to tumor infiltration were evident in a number of sites throughout the rat. The loss of radio-opacity at the proximal head of the femur (a; defined by arrow) is clearly evident using high definition radiograph (Faxitron®) of rat vertebrae and left femur at 21 days post-i.c. injection of MT-1 cells. Lesions within spinal vertebrae were less obvious to demarcate using this technique. Corresponding images using microcomputer tomography x ray of rat vertebrae, with sagittal and transverse views (b) clearly define the metastatic lesions within the bone.

3 Results

3.1 *Rat Model*

3.1.1 *Sensitivity of MT-1 cells to BPD-MA PDT in vitro*

Fluorescence microscopy images taken 45 min post-BPD-MA administration [Fig. 1(a)] confirmed that uptake of BPD-MA into MT-1 cells is ubiquitous, rapid and predominantly targeted to perinuclear organelles within the cell cytosol.

Once inside the cells, the extent of cell kill following BPD-MA mediated PDT in MT-1 cells was quantified *in vitro* using the SRB assay [Fig. 1(b)]. ANOVA statistical analysis confirmed a significant difference ($p<0.001$) between the mean absorbance of the untreated cells versus treated (light and drug) with no statistical difference ($p>0.1$) between untreated wells and wells treated with light or drug only. The

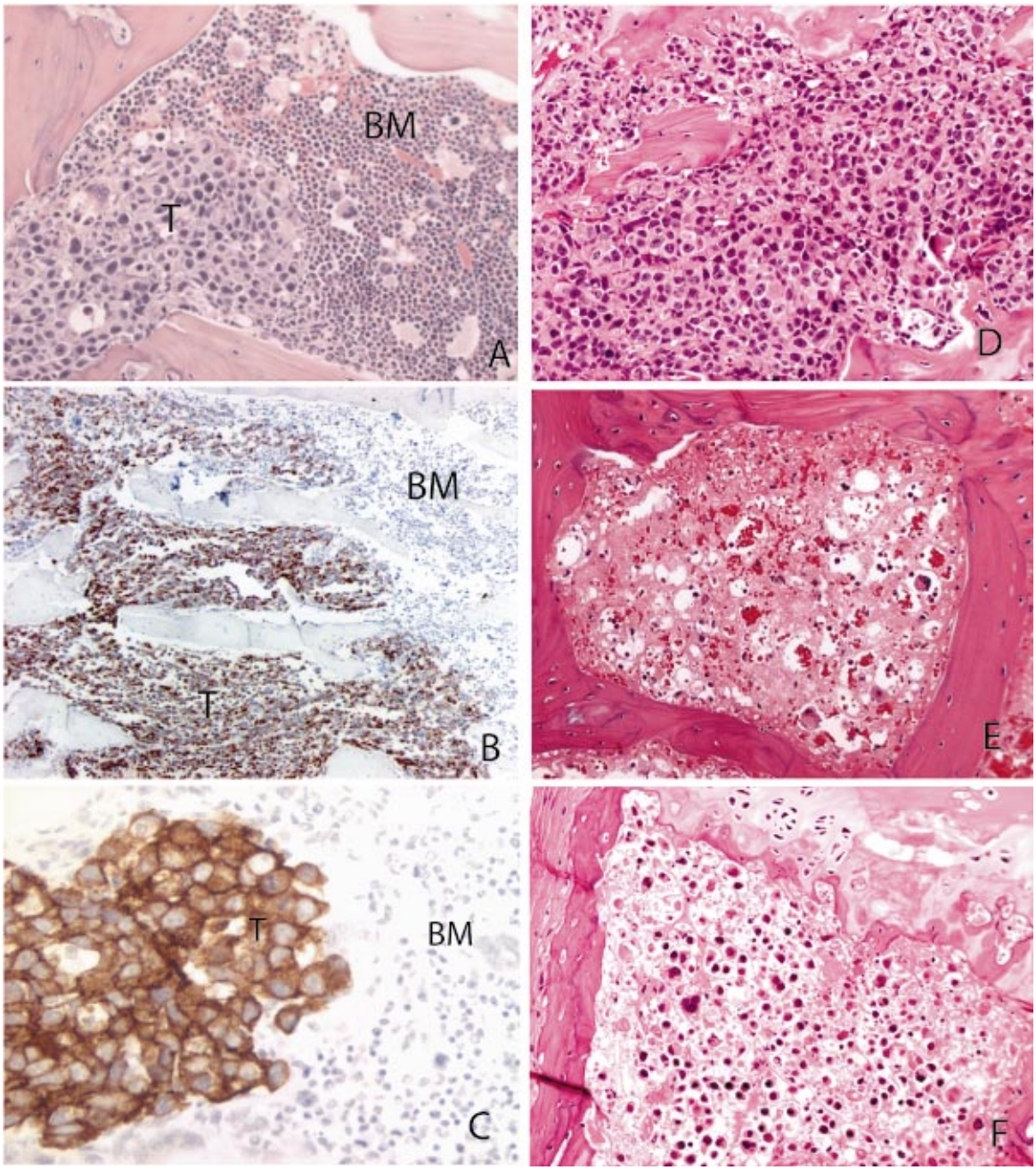

Fig. 5 MT-1 tumor cells (T) are highly conspicuous from surrounding bone marrow (BM) within the vertebrae using haemotoxylin and eosin histological stains (a; magnification is ×10 and d; magnification is ×20) and display high specificity for keratin staining (b; magnification is ×5). MT-1 cells also express high levels of endothelial growth factor receptor (EGFr) which can be immunohistochemically visualized using a human-derived EGFr antibody labeled with horseradish-peroxidase (c; magnification is ×20). The effects of PDT (BPD-MA, 2 mg/mL; i.v.) are clearly evident upon histological analysis with nuclear condensation and blood pooling within the surrounding bone marrow (e and f).

Table 1 Showing the treatment parameters and incidence of paralysis for experimental animals subject to PDT treatment.

Light energy (J)	Vertebral level treated	Drug light interval (h)	Hind leg paralysis	*N*
25	T12	3	0	5
50	T12	3	2 unilateral	5
75	T12	3	1 bilateral	4
100	T12	3	2 unilateral	3
125	T12	3	1 bilateral	2
150	T12	3	3 bilateral	4
150	T12	3	4 bilateral	4
150	T12	24	0	5
150	L4	3	0	5
150	Distal femur	3	0	3
Control*	T12	3	0	3

administration of BPD-MA at a final concentration of 10 or 1 μg/mL followed by a light dose of either 100 or 25 J/cm^2 resulted in comparable cell viability suggesting that the PDT effect was maximal at 1 μg/mL BPD-MA and 25 J/cm^2 light dose.

3.1.2 *BPD uptake in the serum and spinal cord*

Fluorimetry was used to assay the specific uptake of BPD-MA into the spinal cord and blood serum at 15 min, 3 and 24 h post-i.v. injection. Fluorescence intensity versus time (Fig. 2) confirmed the rapid increase in serum drug concentration within 15 min post-injection followed by a steady decline over the next 6 h and returning to base line levels by 24 h. Uptake into the spinal cord was less obvious with a slight increase in intensity at 3 h that cleared by 6 h post-injection. The presence of BPD-MA within the neuronal cell bodies of the spinal cord and the bone marrow of the vertebrae was also evident using fluorescent microscopy at 15 min and 3 h, respectively (not shown). BPD-MA related fluorescence was not evident in either structure at 24 h post-injection.

3.1.3 *The spinal metastases model and quantitative assessment of the BPD-MA induced PDT effect using* MT-1^{Luc} *cells*

Induction of metastatic disease was approximately 70% successful. The mean survival for animals with tumor was 25 days. Four of the animals showed palpable tumors in the femur and tibias as well as the lower mandible. Two animals developed hind leg paralysis secondary to metastatic disease. All animals with tumors became cachexic. The affected animals appeared well until day 18 after which the animals developed rapid weight loss and overt tumors. Faxitron™ x-ray Corp. (Wheeling, IL) indicated lesions within the humerus, femur, and tibia as early as day 14 in some animals [Fig. 3(a)]. However, lesions could not be detected in the vertebrae of any animals by day 21 using Faxitron™. Micro-CT analysis of the thoracic and lumbar spines of these animals showed multiple lytic lesions within the vertebrae [Fig. 3(b)] and tibia (not shown). The mean area of the lytic lesions within the lumbar and thoracic vertebrae was 2.92 and 2.14 mm^2, respectively. The lesions approximated 1/3 of the vertebral body size in both of the lumbar and thoracic vertebrae that were imaged.

Histological analysis of the vertebrae confirmed the presence of osteolytic tumor within the long bones and vertebrae of the affected animals. All animals showed localization of bioluminescent signal to the spine or long bones by day 21. Of the animals used in this study that did not develop paralysis following PDT treatment ($n=20$), the distribution of bioluminescence and hence metastatic disease was comparable for all animals prior to PDT. High signal was obtained from the lumbar and thoracic spine, the humerus, lower mandible, femur, and tibia in addition to the lung. The use of a custom made stereotactic radiolucent jig facilitated localization and targeted treatment of bioluminescent metastases. Targeted lesions treated with 25 J of light with a 3 h drug light interval showed a decrease in tumor growth of 66% compared to that of the control lesions. No effect was seen when light was administered at a 24 h drug light interval or in control animals with light or drug alone. Targeted lesions treated with 150 J of light with a 3 h drug light interval reduced the signal from the targeted site by 87% and decreased tumor growth by 99.8% as compared to control lesions 48 h following treatment (Fig. 4). A total of 13 animals that received PDT in T12 resulted in hind leg paralysis. Parlysis was seen in animals when treated at the 3 h drug light interval at T12 with light doses of between 50 and 150 J but not 25 J. Further, no paralysis was seen at the 24 hr drug light time interval in animals treated with 150 J at T12 or L5 level of the spine. The same was also true for 150 J treatment of the distal femur. Indeed, six animals still showed a diffuse weak bioluminescent signal localized to the treatment site suggesting that viable tumor cells still existed in the bone after treatment. It appears therefore that the photodynamic efficacy is diminished at 24 h post-injection of photosensitizer compared with the 3 h time point. Additionally, four of the animals had high signals within the chest cavity and gross dissection revealed large metastatic tumors within the lung and pericardium. Table 1 details the treatment protocol and incidence of hind limb paralysis for experimental groups.

3.1.4 *The effect of PDT in vertebrae with metastases*

Subsequent histological staining with H&E, keratin and immunohistochemical staining for human EGF-r [see Figs. 5(a)–5(f)] confirmed the presence of human breast cancer cells within the thoracic and lumbar spine. Histological confirmation of tumors within the spine was verified for all of the animals that had metastases present within the spinal cord. Light doses ranging from 25 to 150 J had an ablative effect on both normal bone marrow and tumor tissue. The region of effect ranged from 2.5 to 22 mm in the rostral-caudal dimension. The effect varied in direct proportion to the amount of light given with the greatest effect being seen with 150 J. However, a 75 J light dose administered at a 1 h drug light interval produced a similar effect. Histological analysis of contiguous slices through the rat spine [see Figs. 6(a)–6(d)]

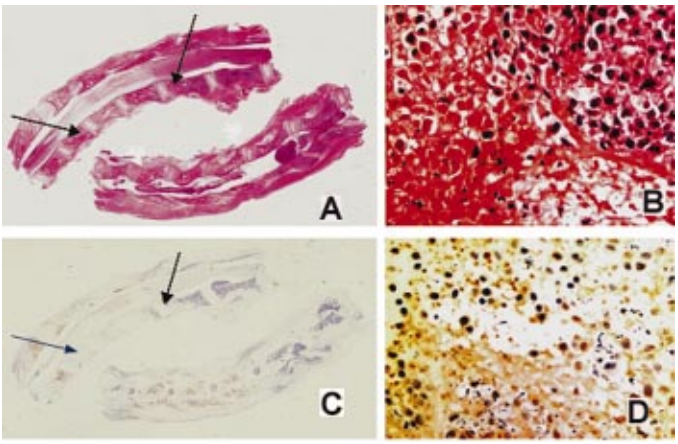

Fig. 6 Brightfield images of rat vertebrae following PDT (150 J, 24 h post-BPD-MA injection). (a) The rostral caudal dimensions of effect (outlined by arrows) are clearly delineated at low magnification (×2.5) after haemotoxylin and eosin staining. (b) The large nucleated tumor cells are evident at higher power at the margins of the necrotic lesion (magnification is ×10). Contiguous slices stained using TUNEL stain reveal the presence of apoptotic cells at the margins of the necrotic lesion at low (c; ×2.5) and high objective magnification (d; ×10).

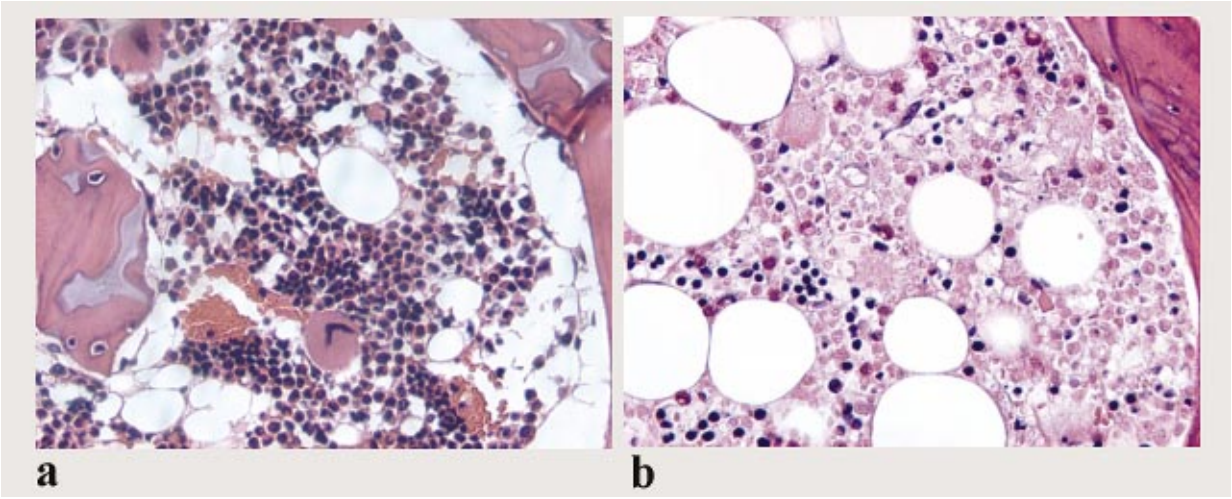

Fig. 9 Histological slice through the pig vertebra pre- (a) and post- (b) BPD-MA PDT. The bone marrow, including osteoclasts, are destroyed with only a few remaining cells in amongst large fat deposits.

confirmed that BPD-MA-PDT with 150 J and 24 h drug/light interval induces wide spread apoptotic cell death at the margins of necrotic lesion [Figs. 6(c) and 6(d)] within the MT-1 metastatic breast cancer 48 h post-treatment.

3.2 *Porcine Model*

3.2.1 *Light transmittance in vertebrae*

Figure 7(a) shows a reconstructed, axial CT image through the pig spine (L1) that clearly reveals the bi-transpedicular placement of treatment and detector probes into the vertebral body. The angle of insertion was critical in order to avoid damaging the spinal cord and to approximate a 90° planar angle between them. Transverse and coronal reconstructions were also analyzed to ensure close approximation between the probe tips in 3-D geometry. Volumetric rendering of the vertebrae using maximum intensity projection [Fig. 7(b)] or shaded surface segmentations [Fig. 7(c)] provided vivid assessment of the probe placement (see arrows) relative to surrounding bony and soft tissue structures, respectively.

The fluence rate of light at the cylindrical diffusing fiber implanted into the pig vertebra (L1 level) was derived using Eq. (1). The average $\Phi(r_n)$ at the necrotic/non-necrotic interface from histological sections was determined to be 4.3 ± 3 mW/cm^2, which for a total treatment time of 36 min, translates into a total delivered fluence of 9.3 J/cm^2. This measurement therefore represents the minimum PDT light dose required to produce necrotic damage within the bone tissues. The radius of necrosis was consistent for most treatments, with $r_n=0.59\pm0.02$ cm $(n=4)$ although since no measurements were made of drug uptake in the treated spines, the actual PDT threshold dose could not be determined. Further, the light dosimetry measurements were difficult to analyze using a standard diffusion model for homogeneous tissues, primarily because of the heterogeneity in tissue structure. However, effective light penetration depths could be estimated for Φ measurements at small source-collection separations. The average penetration depth was 0.16 ± 0.04 cm. An example of the Φ as a function of distance between the detector probe and cylindrical treatment fiber is shown in Fig. 8. An exponential decrease in measured Φ (symbols) is evident for distances of $\leqslant1$ cm with close correlation ($p<0.05$) to the diffusion theory approximation using Eq. (1) as shown by the solid line with a penetration depth, $\delta=0.18$ cm. At separations larger than 1 cm, the analytical fits deviate from the measured values, largely due to the heterogeneity of the spinal tissue. At a separation distance of 1 cm, the Φ decreases by 2 log units and at 2 cm it is <0.01 mW/cm^2. Unfortunately, the considerable variability in measurements from one vertebra to another made averaging these data counterproductive. For qualitative approximation, however, when we apply our treatment parameters to an analytical model previously described by Jacques et al.,[16] we can assume that a doubling of the treatment power will increase the radius of necrosis by 0.205–0.795 cm.

3.2.2 *Effect of PDT in normal pig vertebrae*

The areas of dead cells within bone marrow [Fig. 9(a)] are clearly distinguishable from live tissue [Fig. 9(b)] with mass areas of cellular debris and/or acellularity. Interestingly, on a number of histological sections there was a notable expanse of apoptotic cells beyond the boundaries of necrosis. If substantiated, this may imply that a lower light dose could be valuable as a means of promoting apoptosis over necrosis when treating lesions within bone close to critical structures such as peripheral nerve roots and spinal cord. A similar observation of apoptotic induction at the margins of the targeted area within the vertebrae was also observed in the rat [Figs. 5(c) and 5(d)].

4 Discussion

Breast cancer continues to be the most prevalent cancer accounting for an estimated 211 300 new cases in 2003 (Ref. 17) alone and of those patients that go on to develop systemic malignancies at least 30% will diagnose with spinal metastases during their disease.[18–20] Cancer in bone is often accompanied by very poor prognosis for long-term survival beyond 1–2 years, depending on the primary malignancy. The chronic morbidity associated with spinal metastases, specifically, can be the defining factor predicting survival with intractable back pain due to lesions in one or more vertebral bodies encroaching onto the spinal cord, loss of bowel and bladder function, paresis, and paralysis. As a consequence, the patients' quality of life is often markedly depreciated and declines sharply with increasing longevity. Yet, despite this alarming statistic for mortality and chronic morbidity, the treatment options for such lesions are limited and disturbingly inadequate. In the ambulatory patient the mainstay of treatment is currently RT, however, results of RT for the treatment of spinal metastases have shown that only one third have complete relief of their back pain.[21] The shortfalls of RT are largely twofold. First, that RT is a nondiscerning modality, affecting both normal supporting tissues and tumor tissue alike, which can lead to myelopathy and pronounced fragility within the spine. As a result, the number of treatments as well as the range of radiation dose that can safely be administered for treating spinal tumors is limited. Second, that cells and tissues can rapidly develop resistance to radiation upon subsequent re-treatment(s) thus making the initially prescribed dose quickly ineffective with little option for elevating the dose due to the impending risk of myelopathy and/or bone fracture. Both of these factors contribute to the high incidence of recurrence, an estimated 33%, of patients with spinal metastases,[1,22] which is further exacerbated by an increased longevity of patients with spinal metastases (average survival 2 years with breast cancer, mean 1 year survival of 78%).[23] As recurrence intensifies and lesions become increasing radio resistant, so does the need for spinal surgery. Unfortunately, RT is known to increase the morbidity of surgical intervention by as much as threefold, a procedure that is already associated with a 30–40% risk of morbidity and a 7–16% risk of mortality. Ultimately, alternate approaches for treating tumors within the spine and other bony metastases are urgently needed and we propose that one such potential candidate therapy is PDT.

In order for PDT to be a successful treatment for spinal metastatic lesions, the drug and light combination must be locally targeted to the tumor. In this study we chose BPD-MA as our photosensitizing agent given its propensity to target vasculature and/or tumor cells directly. There are several reports of BPD-MA-PDT in soft tissue tumors in the murine

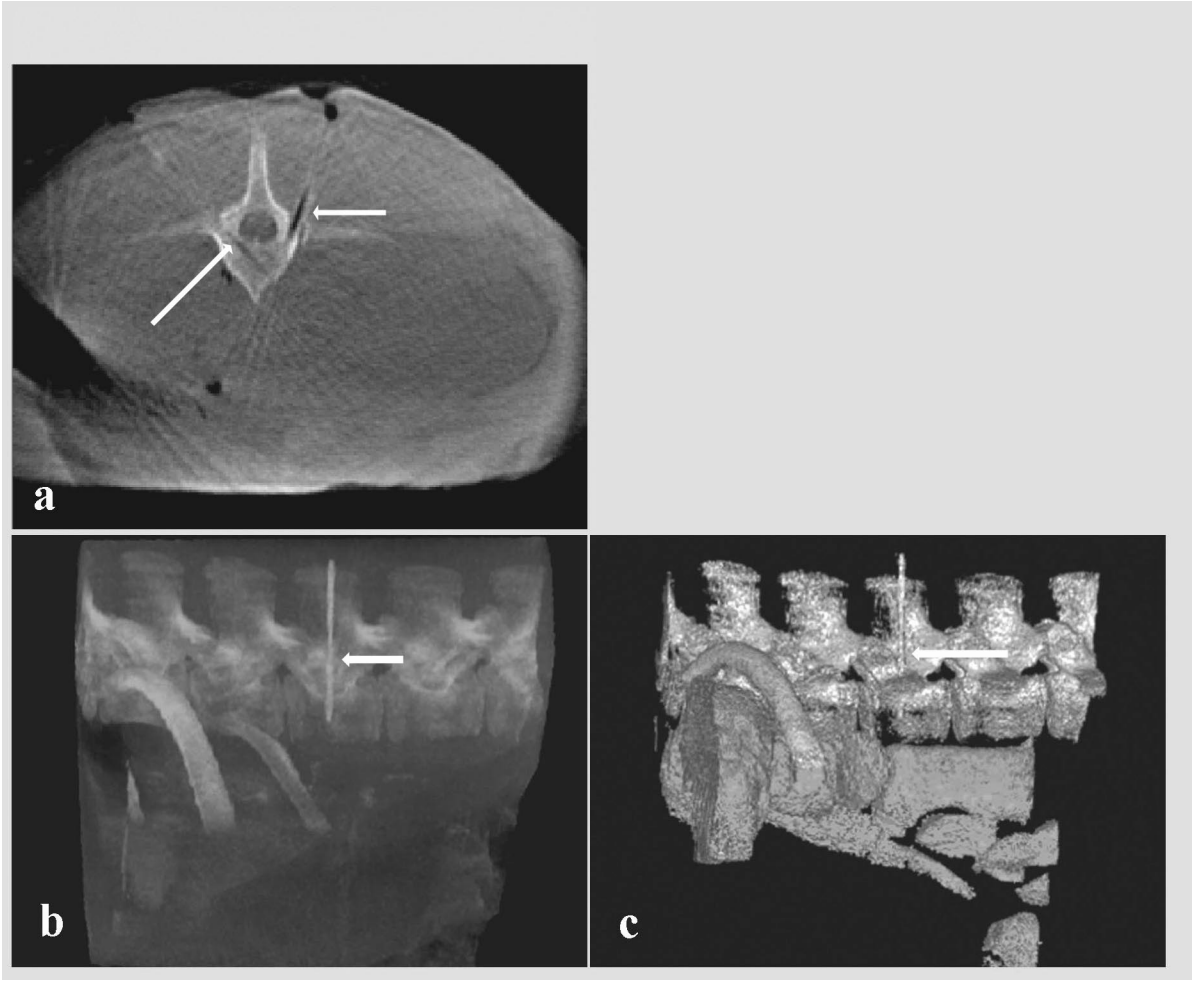

Fig. 7 (a) A CBCT reconstruction in axial plane (512×512×384 at 396 μm voxels) showing the transpedicular trajectory of the probes into the vertebral body of the pig. 3-D volumetric rendering provided clear assessment of the probe position relative to bony structures (b) and soft tissues (c).

model[24–27] as well as in an orthotopic chondrosarcoma[6] and fibrosarcoma tumor models.[28,29] Results from these studies have shown a significant effect at both the 15 min and 3 h drug light interval with 33% of the lesions being completely ablated at 4 weeks post-treatment. A recent study by Koudinova et al. in 2003 (Ref. 30) describes the application PDT using a new vascular targeted photosensitizer, Pd-Bacteriopheophorbide (Tookad™, Steba Biotech, Toussus-Le-Noble, France), to percutaneously treat human small cell carcinoma of the prostate that had been injected directly into the tibia of CD-1, nude mice. The authors report that of those treated for intraosseous tumors, 50% showed complete tumor ablation 2–3 months after treatment. Although not a true representative model for metastatic disease, this paper clearly corroborates the utility of PDT for the treatment of cancers in bone.

To our knowledge there have been no reports until now of PDT use in an *in vivo* metastatic breast cancer model affecting bone and the pharmacokinetics of BPD-MA into bone and the light scattering properties of bone are poorly defined. A number of studies do exist though[31–33] and include Takeuchi et al. in 1997,[34] who, reported that light is attenuated significantly

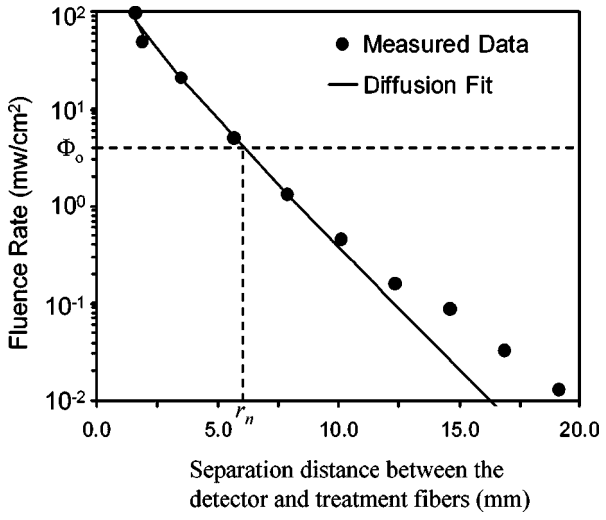

Fig. 8 A plot of decrease in fluence rates in pig vertebra as a function of distance between the detector probe and cylindrical treatment fiber displayed as normalized actual measurements (symbols) and theoretical fit using Eq. (1) (line).

more through cortical bone as compared to cancellous bone, which in itself may prove favorable if the intention is to deliver PDT to a single vertebra without causing collateral damage to the adjacent structures including the spinal cord. This study encompasses the transmittance of light through pig vertebrae as a model for the human spine and describes the delivery of PDT in this model as well as in a small animal, rat model of human metastatic breast cancer. The size of the latter model precludes the placement of optical fibers transpedicularly and para-pedicular insertion would also be difficult.

Consequently, fibers were placed adjacent to the targeted spinal vertebrae and our results confirm that light transmission through metastatically involved rodent vertebrae is impeded minimally by surrounding cortical bone. As such, this study reinforces our hypothesis that PDT can be administered both safely and effectively providing tumor ablation without damaging spinal cord and/or peripheral neurovascular structures. Histology clearly demarcates the boundaries of PDT response revealing substantial ablation of tumor and surrounding bone marrow tissue. The incidence of apoptosis was directly correlative to the metastatic dispersion of MT-1 cells within vertebrae. Further, the influence of PDT on tumor growth kinetics involving differing regiments of BPD-MA and light, was convincingly demonstrated using bioluminescence imaging of MT-1^{Luc} cells *in vivo*. Bioluminescence represents a measure of cellular metabolism. The relative intensity of signal is dependent on the energetic status of the cell and reflects the availability of ATP and molecular oxygen within the cell.[35] Indeed we have recently reported on the use of bioluminescence to monitor the tumor response following PDT.[36] Results in this study reveal a 99.8% decrease in tumor growth 48 h following an acute PDT treatment of 150 J delivered over the course of 16 min. The relative size of response area was correlative to the number of joules of light delivered with a 66% reduction in the tumor growth at 25 J. It was important not to measure the bioluminescent signal during or immediately following PDT as both bioluminescence and PDT are oxygen dependent and therefore a decrease in bioluminescent signal could be interpreted as increased cell death or a reduction in oxygen due to PDT-induced hypoxia.

The effects of PDT on tumors within the thoracic cord were comparable to that of the lumbar spine. The same cannot be said, however, of the surrounding structures, as the presence of spinal cord in thoracic vertebrae but absence in lumbar vertebrae is responsible for the sizable difference in light energy that can safely be delivered into the spine at early time points post-BPD-MA injection without causing paralysis. Indeed, the onset of neurologic sequelae including unilateral and/or bilateral paralysis was only evident following PDT (50–150 J at 3 h) to lesions within the thoracic spine and was not seen following similar treatment in the lumbar region. This observation is important clinically and reiterates the importance of light/drug dosing and the effects of PDT on the neuronal cell bodies within the spinal cord. The target location on the spine and the drug light interval were the major defining factors predicting outcome and response. Our results for BPD-MA biodistribution, although by no means exhaustive and without adequate n number to support statistical conclusions, do provide an inkling as to the pharmacokinetics suggesting that BPD-MA uptake into the spinal cord is negligible and time delayed by $>1–2$ h as compared to the uptake into vertebrae (15 min). This infers that a therapeutic window exists during which PDT can be delivered safely without damage to the spinal cord.

Optical properties within rat vertebrae cannot be extrapolated to that for human vertebrae. For this we chose the pig vertebrae. The vertebral anatomy in pig spine is comparable to that of human thus affording us the opportunity for developing and assessing the trans-pedicular placement of treatment (and detecting) fibers into trabecular bone of the vertebral body (see Fig. 7). The transmittance of light through trabecular bone was measured as fluence with increasing distance between emitting fiber and the detector probe being retracted at 2.5 mm increments out of the vertebral body. The idea that light can travel whether by reflection, scattering or direct transmission, through trabecular bone is not surprising given its cavernous network. Our results imply that 150 J/cm of 690 nm laser light can travel beyond 2 cm from the source fiber, although it is conceivable that this will depend on the extent of blood pooling within the fiber tract and the age of bone. It is also clear that the transmittance of light through bone will not be the same for tumor and dosimetry for treating diffuse metastatic lesions within the spine may require higher energies than predicted from nonlesion vertebrae.

It was also encouraging to note that unlike the rat, the outer layer, cortical bone in pig vertebrae served as very good barriers to light raising the potential for treatment targeted to a single vertebra without risk of damage to adjacent structures. The PDT response in pig was consistent with that in rat with respect to bone marrow ablation and clearly demarcated boundaries of cell death surrounding the treatment fiber. It was also noted that beyond the necrotic zone, a second zone of apoptotic cells was evident in a number of PDT treated vertebra. We have not included a figure showing apoptosis within the pig vertebrae as further studies are necessary to confirm whether the apoptotic induction is, as we suspect, solely attributable to the PDT treatment or whether it is an artifact related to the handling and preparation of the tissue(s) for histology. If verified in subsequent studies, it will be of interest to examine the PDT parameters that induce apoptosis and validate the merits of exploiting apoptotic cell death when targeting lesions close to the spinal cord. In this instance, however, 150 J/cm was implemented as a submaximal, nonthermal light regiment within the center of the trabecular vertebra causing a 0.6 cm radius of necrotic lesion and tissue damage up to 2 cm out from the treatment fiber without damage to the spinal cord. It is likely that higher energies, perhaps administered at the same intensity, could be implemented to provide even larger target response with similar preservation of the spinal cord. Regardless, the observed destruction of bone marrow is clinically advantageous as bone-degrading osteoclasts within the marrow display symbiotic interaction with the growing tumor cells.[37] It is important to note that the integral structure of the bone tissue itself appears to be highly resilient to photodynamic damage. In a report by Meyer et al.[38] the authors describe inducing necrosis within the surrounding soft tissues of the rabbit oral cavity with no effect on the contiguous bony structures. This is an important observation and, despite the fact that jaw is made of flat bone and not cancellous bone, it is one with direct clinical pertinence when

considering the use of PDT in patients where bone may be very weak, such as the elderly.

The practicalities of fiber placement in this current large animal study were critical and rigorous and many of the potential hazards integral to this procedure were quickly realized. Current clinical intervention provides tumor de-bulking by radiation followed by surgical resection when applicable. It is probable that PDT could be added to this arsenal either in adjunct to surgery or as a stand alone therapy with vertebroplasty to provide mechanical stabilization post treatment. The option for fractionated, repeat and/or metronomic PDT[39] regimes can also be considered upon permanent percutaneous implant of optical fibers.

In conclusion, the feasibility of a minimally invasive surgical approach to target spinal metastases using photodynamic therapy has been established in this pre-clinical study. The evaluation of light transmittance through the vertebral body in a pig model reinforces the potential for fiber-based, nonthermal light delivery into bone for targeting lesions up to 2 cm or greater from the treatment fiber without damaging the spinal cord.

Acknowledgments

The authors wish to acknowledge the financial support of QuadraLogic Technologies (QLT, Vancouver, Canada) for costs relating to the study using pigs and the Canadian Breast Cancer Research Alliance IDEAS for funding the rat study. They further thank QLT for providing Verteporfin™. They also recognize Dr. O. Engebraaten of the Norwegian Radium Hospital, Oslo, who kindly provided us with the MT-1, human breast cancer cell line. The last author would finally like to thank Dr. Annie Linn and Sandy LaFrance for their invaluable assistance throughout this study.

References

1. V. Tombolini, A. Zurlo, A. Montagna, E. Notarianni, M. F. Osti, R. M. Enrici, and C. Pirolli, ''Radiation therapy of spinal metastases: results with different fractionations,'' *Tumori* **80**, 353–356 (1994).
2. G. L. Walsh, Z. L. Gokaslan, I. E. McCutcheon, M. T. Mineo, A. W. Yasko, S. G. Swisher, D. S. Schrump, J. C. Nesbitt, J. B. Putnam, Jr., and J. A. Roth, ''Anterior approaches to the thoracic spine in patients with cancer: indications and results,'' *Ann. Thorac. Surg.* **64**, 1611–1618 (1997).
3. S. Milker-Zabel, A. Zabel, C. Thilmann, W. Schenal, M. Wannenmacher, and J. Debus, ''Clinical results of retreatment of vertebral bone metastases by stereotactic conformal radiotherapy and intensity-modulated radiotherapy,'' *Int. J. Radiat. Oncol., Biol., Phys.* **55**, 162–167 (2003).
4. H. Katagiri, M. Takahashi, J. Inagaki, H. Kobayashi, H. Sugiura, S. Yamamura, and H. Iwata, ''Clinical results of nonsurgical treatment for spinal metastases,'' *Int. J. Radiat. Oncol., Biol., Phys.* **42**, 1127–1132 (1998).
5. S. Ryu, F. Fang Yin, J. Rock, J. Zhu, A. Chu, E. Kagan, L. Rogers, M. Ajlouni, M. Rosenblum, and J. H. Kim, ''Image-guided and intensity-modulated radiosurgery for patients with spinal metastasis,'' *Cancer* **97**, 2013–2018 (2003).
6. V. H. Fingar, P. K. Kik, P. S. Haydon, P. B. Cerrito, M. Tseng, E. Abang, and T. J. Wieman, ''Analysis of acute vascular damage after photodynamic therapy using benzoporphyrin derivative (BPD),'' *Br. J. Cancer* **79**, 1702–1708 (1999).
7. Y. Takeuchi, K. Kurohane, K. Ichikawa, S. Yonezawa, M. Nango, and N. Oku, ''Induction of intensive tumor suppression by antiangiogenic photodynamic therapy using polycation-modified liposomal photosensitizer,'' *Cancer* **97**, 2027–2034 (2003).
8. N. Rousset, V. Vonarx, S. Eleouet, J. Carre, E. Kerninon, Y. Lajat, and T. Patrice, ''Cellular distribution and phototoxicity of benzoporphyrin derivative and Photofrin,'' *Res. Exp. Med. (Berl)* **199**, 341–357 (2000).
9. M. Wiedmann, K. Caca, F. Berr, I. Schiefke, A. Tannapfel, C. Wittekind, J. Mossner, J. Hauss, and H. Witzigmann, ''Neoadjuvant photodynamic therapy as a new approach to treating hilar cholangiocarcinoma: a phase II pilot study,'' *Cancer* **97**, 2783–2790 (2003).
10. G. Sutedja and P. E. Postmus, ''The role of photodynamic therapy in the management of stage I/II NSCLC,'' *Lung Cancer* **34**, S35–38 (2001).
11. S. K. Hendren, S. M. Hahn, F. R. Spitz, T. W. Bauer, S. C. Rubin, T. Zhu, E. Glatstein, and D. L. Fraker, ''Phase II trial of debulking surgery and photodynamic therapy for disseminated intraperitoneal tumors,'' *Ann. Surg. Oncol.* **8**, 65–71 (2001).
12. T. R. Nathan, D. E. Whitelaw, S. C. Chang, W. R. Lees, P. M. Ripley, H. Payne, L. Jones, M. C. Parkinson, M. Emberton, A. R. Gillams, A. R. Mundy, and S. G. Bown, ''Photodynamic therapy for prostate cancer recurrence after radiotherapy: a phase I study,'' *J. Urol. (Baltimore)* **168**, 1427–1432 (2002).
13. O. Engebraaten and O. Fodstad, ''Site-specific experimental metastasis patterns of two human breast cancer cell lines in nude rats,'' *Int. J. Cancer* **82**, 219–225 (1999).
14. L. Lilge, C. O'Carroll, and B. C. Wilson, ''A solubilization technique for photosensitizer quantification in ex vivo tissue samples,'' *J. Photochem. Photobiol., B* **39**, 229–235 (1997).
15. T. Kubota, T. Takahara, M. Nagata, T. Furukawa, S. Kase, H. Tanino, K. Ishibiki, and M. Kitajima, ''Colorimetric chemosensitivity testing using sulforhodamine B,'' *J. Surg. Oncol.* **52**, 83–88 (1993).
16. S. Jacques, ''Light distributions from point, line and plane sources for photochemical reactions and fluorescence in turbid biological tissues,'' *Photochem. Photobiol.* **67**, 23–32 (1998).
17. L. Riss, *SEER Cancer Statistics Review*, National Cancer Institute, Bethesda, MD (1975–2000).
18. J. A. Ortiz Gomez, ''The incidence of vertebral body metastases,'' *Int. Orthop.* **19**, 309–311 (1995).
19. H. Tatsui, T. Onomura, S. Morishita, M. Oketa, and T. Inoue, ''Survival rates of patients with metastatic spinal cancer after scintigraphic detection of abnormal radioactive accumulation,'' *Spine* **21**, 2143–2148 (1996).
20. D. A. Wong, V. L. Fornasier, and I. MacNab, ''Spinal metastases: the obvious, the occult, and the impostors,'' *Spine* **15**, 1–4 (1990).
21. C. M. Faul and J. C. Flickinger, ''The use of radiation in the management of spinal metastases,'' *J. Neuro-Oncol.* **23**, 149–161 (1995).
22. N. Sundaresan, G. V. Digiacinto, J. E. Hughes, M. Cafferty, and A. Vallejo, ''Treatment of neoplastic spinal cord compression: results of a prospective study,'' *Neurosurgery* **29**, 645–650 (1991).
23. R. Wedin, H. C. Bauer, and L. E. Rutqvist, ''Surgical treatment for skeletal breast cancer metastases: a population-based study of 641 patients,'' *Cancer* **92**, 257–262 (2001).
24. A. M. Richter, E. Waterfield, A. K. Jain, B. Allison, E. D. Sternberg, D. Dolphin, and J. G. Levy, ''Photosensitising potency of structural analogues of benzoporphyrin derivative (BPD) in a mouse tumor model,'' *Br. J. Cancer* **63**, 187–193 (1991).
25. S. Gluck, A. Chadderton, and A. D. Ho, ''The selective uptake of benzoporphyrin derivative mono-acid ring A results in differential cell kill of multiple myeloma cells in vitro,'' *Photochem. Photobiol.* **63**, 846–853 (1996).
26. T. Momma, M. R. Hamblin, H. C. Wu, and T. Hasan, ''Photodynamic therapy of orthotopic prostate cancer with benzoporphyrin derivative: local control and distant metastasis,'' *Cancer Res.* **58**, 5425–5431 (1998).
27. A. M. Richter, E. Waterfield, A. K. Jain, A. J. Canaan, B. A. Allison, and J. G. Levy, ''Liposomal delivery of a photosensitizer, benzoporphyrin derivative monoacid ring A (BPD), to tumor tissue in a mouse tumor model,'' *Photochem. Photobiol.* **57**, 1000–1006 (1993).
28. K. Kurohane, A. Tominaga, K. Sato, J. R. North, Y. Namba, and N. Oku, ''Photodynamic therapy targeted to tumor-induced angiogenic vessels,'' *Cancer Lett.* **167**, 49–56 (2001).
29. L. Cincotta, D. Szeto, E. Lampros, T. Hasan, and A. H. Cincotta, ''Benzophenothiazine and benzoporphyrin derivative combination phototherapy effectively eradicates large murine sarcomas,'' *Photochem. Photobiol.* **63**, 229–237 (1996).
30. N. V. Koudinova, J. H. Pinthus, A. Brandis, O. Brenner, P. Bendel, J. Ramon, Z. Eshhar, A. Scherz, and Y. Salomon, ''Photodynamic therapy with Pd-Bacteriopheophorbide (TOOKAD): successful in vivo treatment of human prostatic small cell carcinoma xenografts,'' *Int. J. Cancer* **104**, 782–789 (2003).

31. M. Firbank, M. Hiraoka, M. Essenpreis, and D. T. Delpy, ''Measurement of the optical properties of the skull in the wavelength range 650–950 nm,'' *Phys. Med. Biol.* **38**, 503–510 (1993).
32. S. Tauber, R. Baumgartner, K. Schorn, and W. Beyer, ''Light dosimetric quantitative analysis of the human petrous bone: experimental study for laser irradiation of the cochlea,'' *Lasers Surg. Med.* **28**, 18–26 (2001).
33. A. O. Ugnell and P. A. Oberg, ''The optical properties of the cochlear bone,'' *Med. Eng. Phys.* **19**, 630–636 (1997).
34. A. Takeuchi, R. Araki, S. G. Proskurin, Y. Takahashi, Y. Yamada, I. J. Shii, S. Katayama, and A. A. Itabashi, ''New method of bone tissue measurement based upon light scattering,'' *J. Bone Miner. Res.* **12**, 261–266 (1997).
35. L. F. Greer and A. A. Szalay, ''Imaging of light emission from the expression of luciferases in living cells and organisms: a review,'' *Luminescence* **17**, 43–74 (2002).
36. E. H. Moriyama, S. K. Bisland, L. Lilge, and B. C. Wilson, ''Bioluminescence monitoring of photodynamic therapy response of rat gliosarcoma in vitro and in vivo,'' *Proc. SPIE* **4952**, 76–81 (2002).
37. T. Okada, S. Akikusa, H. Okuno, and M. Kodaka, ''Bone marrow metastatic myeloma cells promote osteoclastogenesis through RANKL on endothelial cells,'' *Clin. Exp. Metastasis* **20**, 639–646 (2003).
38. M. Meyer, P. Speight, and S. G. Bown, ''A study of the effects of photodynamic therapy on the normal tissues of the rabbit jaw,'' *Br. J. Cancer* **64**, 1093–1097 (1991).
39. S. K. Bisland, L. Lilge, A. Lin, and B. C. Wilson, ''Metronomic photodynamic therapy (mPDT) for intracranial neoplasm: physiological, biological, and dosimetry considerations,'' *Proc. SPIE* **5142**, 9–17 (2003).